Am J Clin Exp Urol 2026;14(2):45-54
www.ajceu.us /ISSN:2330-1910/AJCEU0170543

*Original Article*

# Characterization of renal pelvis compliance and outflow resistance during ureteroscopy of the ex-vivo human kidney

Rainer Leuschke[1], Alex Gong[1], Austin J Baird[1], Aditi Ray[2], Robert M Sweet[1]

*[1]Division of Healthcare Simulation, University of Washington, Seattle, WA, USA; [2]Boston Scientific, Marlborough, MA, USA*

Received December 5, 2025; Accepted March 6, 2026; Epub April 15, 2026; Published April 30, 2026

**Abstract:** Introduction: Elevated intrarenal pressure during ureteroscopy has been linked to complications during recovery from stone removal surgery. Intrarenal pressure depends on irrigation flow rate, inflow and outflow resistance, and kidney compliance. These have been examined for porcine models in the literature. In this study, we report on the experimental method and results of characterizing compliance and outflow resistance in human cadaveric kidneys. Methods: To characterize compliance a catheter is inserted retrograde into the renal collecting system and sealed at the UPJ. Pressurized irrigation fluid is then allowed to flow into the renal pelvis. Pressure and flow are recorded over time, representing a measure of compliance. To characterize outflow resistance a UAS is inserted into the ureter and a ureteroscope placed. Inflow is increased over time and pressure and outflow recorded. Results: The resulting compliance curves show a high variability between specimens. Anatomical differences and initial volume are significant contributing factors. We show that non-dimensionalizing the data with respect to a measure of volume allows us to fit a single non-linear compliance model to the data. Our outflow testing shows that with consistent placement of devices, outflow resistance is primarily a function of device parameters and largely independent of the specimen anatomy. We determined an outflow resistance of 8.1 mmHg/(ml/min) ($\sigma$ = 1.6) for UAS size 10/12 F, 0.73 mmHg/(ml/min) ($\sigma$ = 0.05) for size 11/13 F and 0.18 mmHg/(ml/min) ($\sigma$ = 0.04) for size 12/14 F. Conclusion: The compliance results for human kidneys add a critical data set that enables more accurate modelling of the mechanics of processes involved in stone removal. The outflow data similarly provides critical parameters for modelling the mechanics of ureteroscopic procedures and confirms that this characteristic is primarily driven by surgical device parameters.

**Keywords:** Ureteroscopy, ex vivo experiments, intrarenal pressure, kidney compliance, outflow resistance

## Introduction

Laser lithotripsy is a common method for removal of small and medium sized kidney stones. A flexible ureteroscope is passed through the urethra, bladder and ureter into the kidney. A laser fiber is inserted through the working channel of the scope, and laser light is used to break up the stones. Stone fragments and dust are cleared out directly through basketing, are washed out with the irrigation fluid or pass naturally after the procedure. Fluid irrigation is used to aid in visualizing the ureter and renal spaces and manage heat generated by the laser. Irrigation fluid is discharged through the ureter with the flow path restricted to the space between ureteroscope and ureteral wall, or interior of the ureteral access sheath (UAS) if one is used. This flow restriction is characterized by the outflow resistance. A significant restriction can lead to potentially damaging pressure buildup in the kidney [1-4].

Mechanical characterization of tissue is used in a variety of different research domains including AR/VR medical simulation training [5], disease characterization [6, 7], and medical device development [8, 9]. Understanding the response of the surrounding tissue to any device it is interacting with helps prevent severe injury and harm to the patient [10]. To that end various studies have begun to quantify mechan-

https://doi.org/10.62347/YZCG3056

ical properties of renal tissue including analyzing failure thresholds for maximum stress/strain, and strain energy density (SED) of the whole-infused rhesus monkey kidney [11], measuring the tension, compression, and shear mechanical properties of the porcine kidney [12, 13], studies of the mechanical behavior of cadaveric human kidneys under axial and transversal loadings [14]. Notably, none of these studies quantify internal in-tact human kidney tissue Experimental tests have tried to measure internal tissue through extraction or aspiration techniques (for human and porcine kidneys) to understand different strain rates [15-17]. For these studies, the aspiration process recorded by the camera was used to obtain the mechanical properties of kidney tissue by fitting a finite element simulation to experimental data. A novel approach using ultrasound to asses kidney mechanical properties has been demonstrated by [18]. The studies cited above focus on characterizing the mechanical properties of the renal parenchyma. Due to the difficulties of collecting ex-vivo organs for testing and the obvious ethical limitations of internal in-vivo testing, there is a paucity of renal tissue characterization data, especially pertaining to internal measurements of an in-tact kidney.

To properly analyze patient safety in the context of laser lithotripsy, we must understand the mechanical characteristics of the pyelocalyceal system and the interplay of intrarenal pressure, irrigation fluid flow and thermal loading from laser activation in the human kidney. Mechanical properties of the parenchyma play a significant role in that the tissue mechanically constrains the renal pelvis and calyces. The aggregation of experimental data is critical for construction of predictive models that describe the relationship between irrigation inflow, outflow, and intrarenal pressure. Prior studies have developed lumped parameter models to describe these relationships [19, 20]. Inflow resistance, kidney compliance, and outflow resistance are critical parameters of these models and have been examined experimentally. These experiments have largely been limited to porcine models [20-22]. Compliance of the kidney is critical to the transient response to input pressure changes. Oratis, et al. [19] proposed a linear model, while Williams, et al. [20] showed that an exponential model is a better match with experimental data. Rehman, et al. [23], Kim, et al. [24], Marom, et al. [25] and Williams, et al. [20] investigated outflow resistance supported by experimental data. Informing model design and parameterization is critical in performing validated computational experiments. Tissue biomechanical characterization is one important component of that work.

Beyond computational modeling, many other domains are beginning to construct realistic kidney phantoms, with many of these synthetic constructs needing accurate biomechanics to be synthesized properly [26-28]. Biomimetic material construction of the glomerulus, for example, has the potential to improve understanding of pathogenesis of kidney disease, enabling therapeutic investigations [29]. Without proper biomechanics, fluid flows and dynamic responses to fluidic stimuli would be inaccurate. The collecting system, including the ureter, plays an important role in the formation of the urine, which is a vital component and function of the kidney. Understanding the biomechanics of the collecting system improves these synthetic surrogate models, thus improving surgical planning, disease and therapeutic interventions, and aids in construction of in-vitro models [30]. To date, a full understanding of the human collecting system has been omitted from mechanical studies, with all prior work focusing on the ureter [28], or only measuring animal models [31]. The innovation of this study is that we are quantifying the mechanical properties of the human collecting system through perfusion of the space, measuring the fluid pressure induced by this fluid buildup. In this work, we are aiming to characterize kidney compliance and outflow resistance using human ex-vivo kidney specimens. Predictive models and synthetic phantoms for kidney mechanical and thermal behavior during ureteroscopy will ultimately be a helpful tool in validating new approaches, settings, and devices [27, 32-34]. Characterization of kidney behavior is a critical step in developing these models.

## Materials and methods

Experiments to determine outflow resistance and compliance were performed on twenty ex-vivo cadaveric human kidneys as well as four

kidneys in two in-situ human cadavers. For ex-vivo specimens, healthy kidneys were recovered from fresh, unfixed organ donors. The kidneys were stored in University of Wisconsin solution at 4°C and tested within 72 hours of cross-clamp. The ex vivo kidneys were on a kidney pump until being packaged and shipped to the CREST lab after being declined from transplant hospitals. The duration of the study was over a period of 6 months. Procurement and testing of cadaveric specimens were deemed institutional review board exempt by the University of Washington's Human Subject Division (HSD 52692). All specimens were legally authorized by the family of the deceased and donated for research purposes. The ex vivo specimens were obtained from LifeCenter Northwest. The two in-situ cadavers were procured from ScienceCare.

Testing of specimens A-S was carried out at room temperature. Specimens T-Y were tested at body temperature. Outflow resistance data was collected for specimens K-S only, all at room temperature.

*Compliance testing setup*

For compliance testing, the connective tissue around the kidney was resected to allow easy access to the ureter and venous and arterial vessels. A 7F dual lumen catheter was inserted into the ureter with the catheter openings near the tip just past the UPJ. A zip tie was placed just below the UPJ to secure the catheter in place and prevent leakage through the ureter between catheter and interior ureter wall. Venous and arterial vessels were clamped as close to the capsule as possible using two large hemostats. 0.9% Saline solution with added green dye was chosen as the irrigation fluid. The irrigation fluid was pressurized with an inflatable pressure sleeve to 200 mmHg supply pressure. For compliance testing, flow was regulated manually using a roller clamp to a flow rate of 3 ml/min ±10%. This flow rate was determined to be suitable in initial testing on specimens A and B. The irrigation fluid was supplied through the larger lumen of the catheter into the kidney. Data was recorded until the intrarenal pressure reached 100 mmHg, or the pressure rise slowed significantly. The kidney compliance test was run 3 times on each kidney with a 20 min rest period between runs. A Sensirion SLS1500 flow meter, connected in the supply path, was used to measure the flow rate. Fluid volume was calculated from the recorded inflow. The sensing lumen of the catheter was connected to a custom pressure transducer board with Honeywell MPRLS sensors to obtain pressure measurements from inside the renal pelvis. All data was recorded at a 100 ms interval.

*Outflow resistance testing setup*

Specimens K-S were tested both for compliance and outflow resistance. For each of these specimens, the outflow resistance testing was performed after compliance testing. For this test, a ureteral access sheath (UAS) was inserted through the ureter into the renal pelvis with the tip just past the UPJ. A zip tie was used to secure the UAS to the ureter. UAS sizes 10/12 F, 11/13 F, and 12/14 F were used in separate test runs. A Boston Scientific LithoVue Elite ureteroscope (9.5F) was then inserted with its tip just past the end of the UAS. The ureteroscope tip contains the working port where irrigation fluid flows into the renal space. It also contains the pressure transducer for intrarenal pressure measurements. Venous and arterial vessels were clamped as close as possible to the capsule using two large hemostats. The irrigation fluid supply was connected to the scope fluid port with supply pressure set to 25 mmHg. At the start of the test run, the fluid supply was opened fully. System pressure was increased stepwise every 60 s, by 25 mmHg up to 100 mmHg and subsequently by 50 mmHg up to 300 mmHg. The irrigation fluid return flow passes from the renal pelvis between the scope and inner wall of the UAS. The outflow is captured in a vessel positioned on top of an A&D EK-3000i precision scale. Scale data output was recorded at a 100 ms interval. Outflow rate is calculated from scale weight. The pressure in the renal pelvis was recorded at a ~250 ms interval using the integrated pressure transducer of the LithoVue Elite ureteroscope and the StoneSmart console.

*Statistical analysis*

An exponential model of the form $P_{ilp} = a \times (e^{bV}-1)$ was shown to be suitable to model compliance behavior by Williams [14]. Due to the clear spread of the specimen data, we compute confidence intervals of the nonlinear fit using

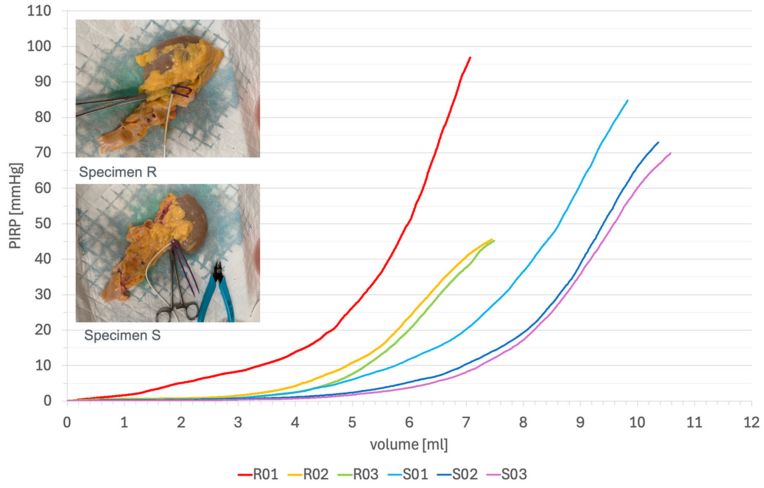


**Figure 1.** Renal pelvis compliance plot for specimens R and S.

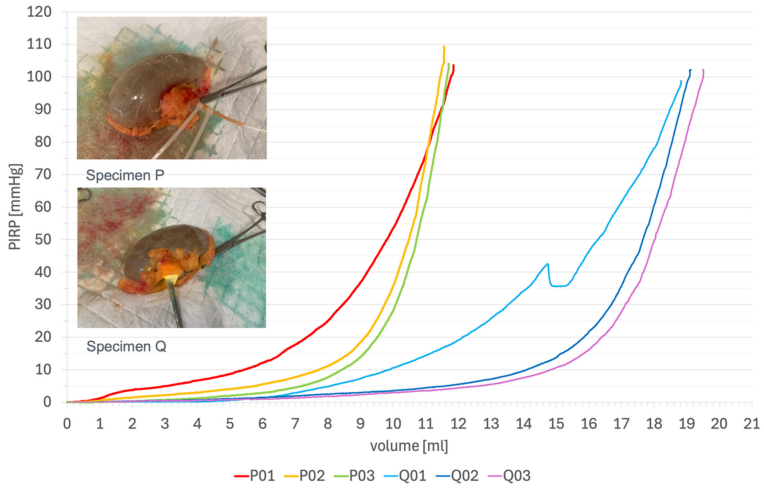


**Figure 2.** Renal pelvis compliance plot for specimens P and Q; data specimen Q is illustrating the effect of an extrarenal pelvis.

the delta method which assumes some randomness in the predicted coefficient values during nonlinear regression (here using least-squares). We compute the variance interval of the regressed parameters by computing the Jacobian and variance-covariance matrix, where we can define this variance by:

$$Var(G(\beta)) \sim \nabla G(\beta) Cov(\beta) \nabla G(\beta)'$$

Here, beta is a vector of parameters that we fit using non-linear least squares, and the prime indicates the transpose of the gradient matrix. We are performing a second order approximation of the variance of the parameters using a Taylor series of the exponential function we are fitting here. Thus, for a given exponential model we may sample a specific model by sampling each fit parameter for the variance and distribution, computed here.

## Results

### *Compliance testing results*

Over the duration of this study, we were able to obtain test data for a significant number of kidneys. The average age of the specimen donors was 62.5 years ($\sigma$ = 12.2). The recorded time series data was trimmed to only include the portion of increasing pressure. The flow rate measurement was converted to a volume estimate for this data. Plotting intrarenal pressure vs fluid volume provides the compliance curve of the renal pelvis. The compliance plot for two specimens, three test runs each, is shown in **Figure 1**. A conditioning effect was generally noted for most specimens where the second and third run show a larger volume and more compliant behavior. In several specimens, we observed second and third runs that failed to reach the same pressure levels as the initial run, as shown here for specimen R (see **Figure 1**).

An extrarenal pelvis is a normal anatomical variation where the renal pelvis is located outside the renal sinus and occurs in ~10% of patients [35]. We observed this in at least one kidney (see **Figure 2**). The compliance plot shows a distinctive dip when the renal pelvis expands into the space outside the renal sinus. Subsequent runs did not show this behavior as the renal pelvis never fully returned to its original configuration. A significantly larger volume of the renal pelvis is observable.

The exponential model of the form $P_{ilp} = a \times (e^{bV}-1)$ as discussed above provided a good fit

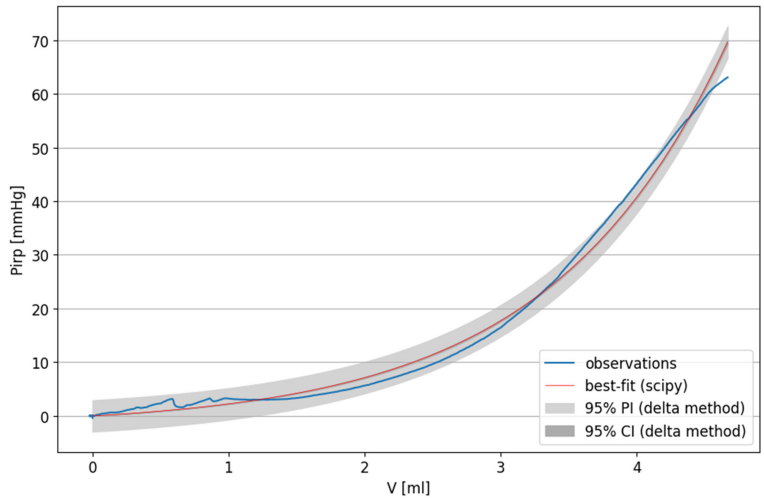


**Figure 3.** Non-linear regression curve fit to an exponential model with confidence interval and prediction interval for specimen X.

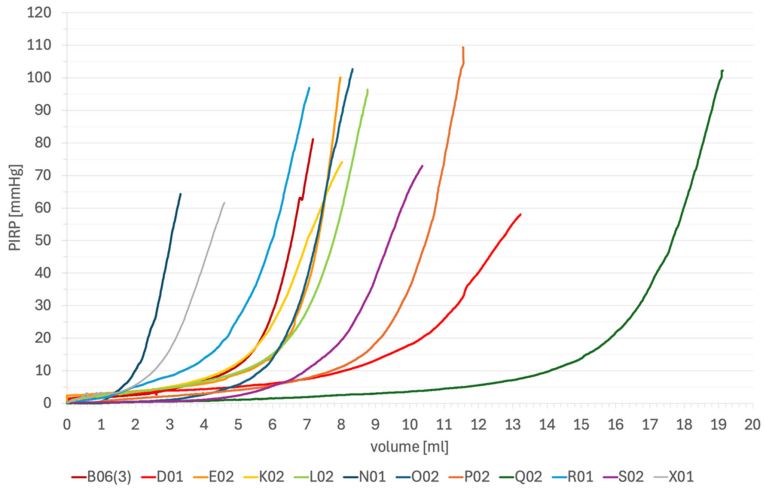


**Figure 4.** Compliance plot for specimens with pressure performance > 50 mmHg, testing at 3 ml/min fill rate.

for our specimen data. **Figure 3** shows the regression fit to the compliance data for specimen X using non-linear regression with SciPy. The confidence interval during fit was computed using the delta method as described above. The resulting model for specimen X, for a given mean sample parameter value, is:

$P_{irp} = 1.92 \times (e^{0.77V}\text{-}1)$

Where $P_{irp}$ is the intrarenal pressure in mmHg, and V is the volume in ml. R-squared is 0.9934. Standard error of regression is 1.4863.

A large portion of the specimens did not reach our target pressure of 100 mmHg, including all four in-situ specimens. About half of the specimens demonstrated a reproducible pressure rise above 50 mmHg. This was chosen as a threshold for further modelling. Specimens that did not meet this criterium were not further considered. **Figure 4** shows the compliance plots of the specimens that meet the 50 mmHg pressure performance criteria. Significant variability across the samples can be observed. The difference in initial volume appears to be the dominant cause of this variability.

To obtain a single predictive model, the data was non-dimensionalized using the volume at a threshold pressure. This eliminates the impact of initial volume of the renal space on the compliance curve. Croghan, et al. [2] determined the baseline intrarenal pressure in an in vivo study to be 16.45 mmHg (σ = 5.99). We chose a threshold value of $P_{th}$ = 20 mmHg as sufficiently high that the renal space has been filled, and further inflow results in steep increase in pressure based on strain in the tissue. The exponential model was fitted to the non-dimensionalized data using non-linear regression with SciPy (see **Figure 5**). Confidence and prediction intervals were determined using the delta method as described above. The resulting model is:

$P_{irp}/P_{th}=0.06\times(e^{3.09V/V_{th}}\text{-}1)$

Where $P_{irp}$ is the intrarenal pressure, $P_{th}$ is the threshold pressure, V is the volume in ml and $V_{th}$ is the volume at threshold pressure. R-squared is 0.8908. Standard error of regression is 0.4015.

For a visual comparison the compliance test data were overlayed with curve fit results for ex vivo porcine models from Williams, et al. [20]

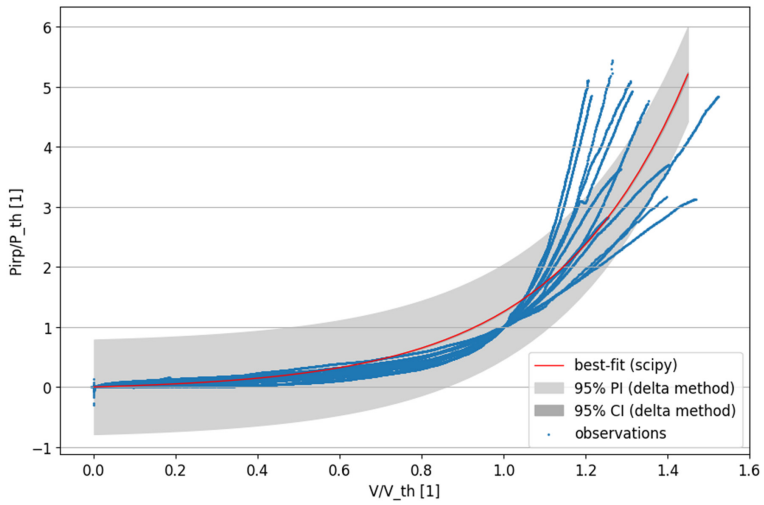


**Figure 5.** Non-linear regression curve fit to an exponential model for all specimens with > 50 mmHg pressure performance; data non-dimensionalized with $P_{th}$ = 20 mmHg.

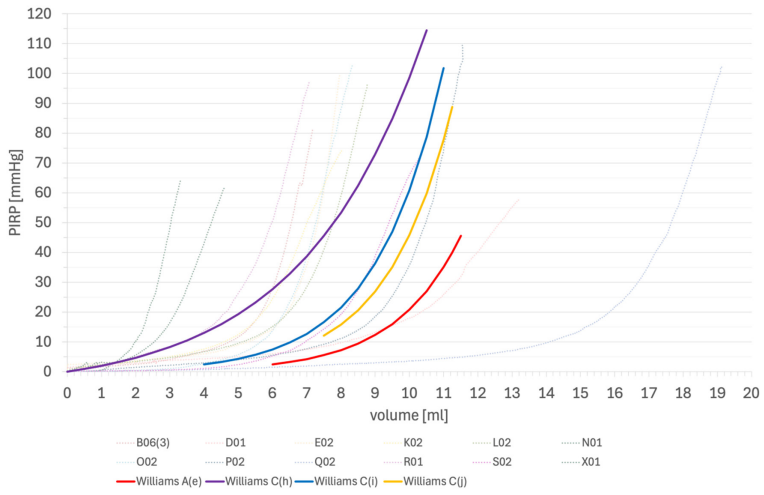


**Figure 6.** Comparison of compliance test results for porcine ex-vivo testing by Williams [14] and human ex-vivo specimens of this study.

in **Figure 6**. Note that mass/volume in the Williams data was initialized for the first run of a series of tests. Curve A(e), C(i) and C(j) are therefore offset horizontally.

*Outflow resistance testing results*

**Figure 7** shows the time series pressure trace for outflow resistance testing on a set of kidneys recorded by the StoneSmart console. This data is trimmed and aligned with recorded data from the scale and the system pressure. For each step in system pressure, the intrarenal pressure and outflow rate are determined as an average over the last 20 sec of constant pressure. Outflow resistance is the ratio of intrarenal pressure and outflow rate. A linear model can be fitted to the test data to determine the outflow resistance (see **Figure 8**). Results for specimen K through S are shown in **Figure 9**.

Outflow resistance for UAS size 10/12 F was determined to be: 8.1 mmHg/(ml/min) (σ = 1.6), 11/13 F: 0.73 mmHg/(ml/min) (σ = 0.05), 12/14 F: 0.18 mmHg/(ml/min) (σ = 0.04).

## Discussion

We sought to characterize collecting system mechanical behavior for irrigation during ureteroscopy in human ex-vivo kidney specimens. Lump-parameter models were previously developed by Oratis, et al. [19] and Williams, et al. [20]. The transient response to input pressure changes is significantly impacted by the compliance of the pyelocalyceal system. Work to characterize compliance has largely been done on in-vivo [21] and ex-vivo [20] porcine models. The compliance data we obtained from ex-vivo human kidneys showed similar compliance behavior to the porcine specimens from [20] as shown in **Figure 6**. An exponential model, proposed by Williams, provides a good fit to the human data. We observed significant variability between compliance curves for individual specimens. We suggest that key factors are anatomical variability, specimen quality and experimental setup limitations.

The compliance data shows that the specimens that were tested successfully have a significant spread in initial volume of the renal collecting system. All reviewed studies of porcine renal system compliance provide data for a rel-

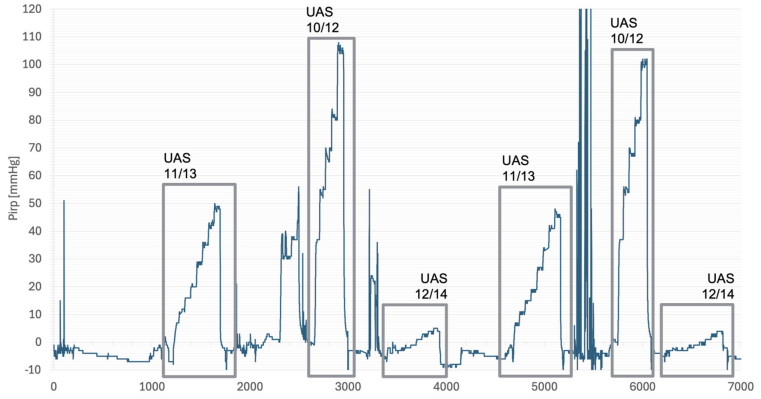


**Figure 7.** Time series pressure trace for outflow resistance testing for specimens N and O.

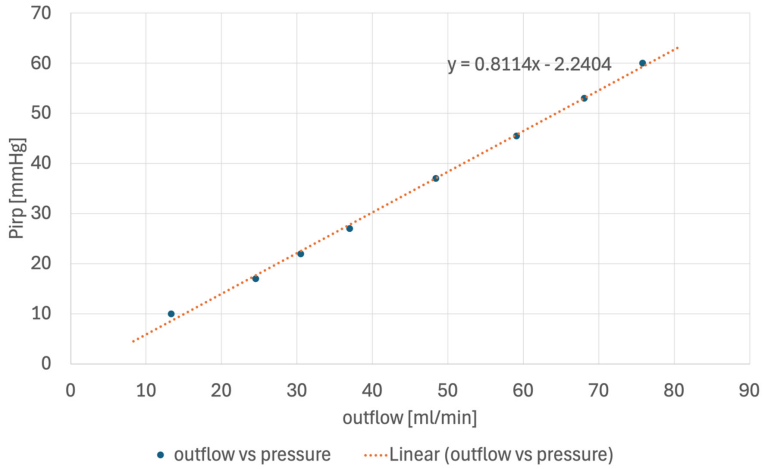


**Figure 8.** Linear regression fit for a linear outflow resistance model for specimen Q with UAS 11/13.

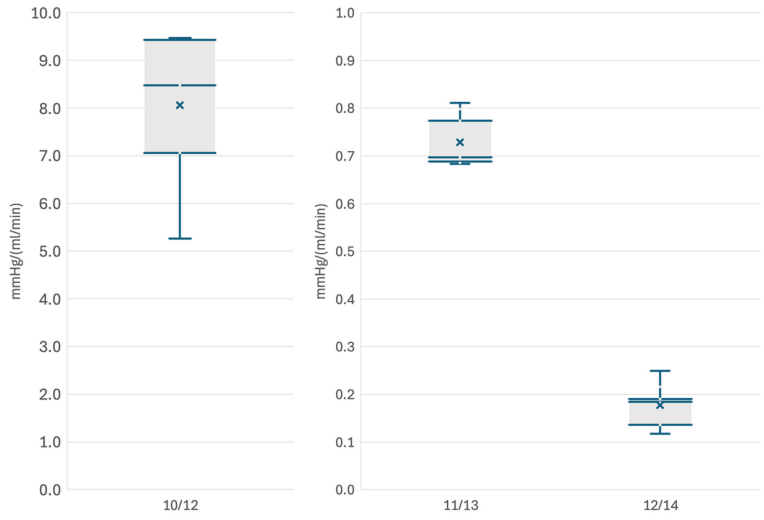


**Figure 9.** Outflow resistance for specimens K through S using UAS sizes 10/12 F, 11/13 F and 12/14 F.

atively small number of samples. This makes it challenging to draw conclusions about anatomical variability for these animal models. To account for variability in specimen size, we non-dimensionalized the data using the volume at a fixed threshold pressure of 20 mmHg. The non-dimensionalized data was fit to an exponential model.

For a significant number of specimens, some form of leakage was evident in the data and visible on the renal capsule due to coloration by the irrigation fluid. Leakage caused the renal pressure to level off at pressures lower than expected. We attempted to minimize pyelovenous and pyeloarterial backflow by clamping off vessels at the capsule but could not control leakage into internal vasculature and interstitial spaces in the capsule. Some of the leakage is thought to be associated with the lack of physiologically accurate blood pressure and vascular tone. The high age of specimen donors and time delay between harvesting and experiment are also likely contributors to the quality of the specimens. The ex-vivo kidneys obtained for these experiments are perfused with a kidney perfusion pump after harvesting until they are rejected for transplanting. In doing so, it reduces the potential for clots in the renal microvasculature. A small number of kidneys showed a significant deterioration of their ability to support increased renal pressure after the first run of the experiment. Similarly, some specimens did not support increased renal pressure at the

given flow rate from the start. This is thought to have been caused by forniceal rupture resulting in significant internal leakage of irrigation fluid. A small number of specimens were tested at body temperature. Only a single compliance test of these met the performance threshold. The data from this test fell well within the results range of room temperature tests.

The outflow resistance for irrigation fluid during ureteroscopy is a key parameter driving the intrarenal pressure. It impacts both transient and steady state responses. When a UAS is in use, the outflow resistance is largely dependent on the size of the ureteroscope and size and length of UAS. The compliance of the kidney is not a factor during steady state irrigation, and outflow resistance is determined as the ratio of renal pressure and flow rate. Data from nine specimens showed consistent linear behavior and small variability for all sizes of UAS. While the compliance data for the same specimens showed significant variability, the outflow resistance did not. Outflow resistance is shown to be largely independent of anatomical characteristics. It is driven primarily by the geometry of the selected devices. Outflow resistance has been previously quantified in an in-vitro study for multiple devices [24]. For a 9.5F ureteroscope with UAS size 13/15F it was determined to be 0.15 mmHg/(ml/min), and 0.81 mmHg/(ml/min) for UAS size 11/13F. These results align well with our findings.

## Conclusion

The data collected in this study is a valuable asset in building predictive dynamic models and synthetic phantoms of the renal pelvis under ureteroscopy and other procedures. Overall volume and anatomical structure of the collecting system appear to be critical parameters in driving dynamic behavior of the kidney. A key limitation in our approach to characterizing dynamic compliance of the renal pelvis was the observed internal leakage of irrigation fluid by a significant portion of our specimens. While our approach gives us a useful estimate of volume, an imaging approach to capturing volume and structure is likely to support higher fidelity models. Incidentally the requisite type of imaging data can be captured in surgical planning for stone procedures. The imaging data may eventually be evaluated with traditional or AI tools to build personalized dynamic models of a patient's collecting system that can ultimately be leveraged by the surgical team to maximize patient safety. Similarly, this data will be a significant input in the design of synthetic phantoms suitable for validating approaches, settings and devices across a range of anatomical variation.

## Acknowledgements

The authors would like to acknowledge the support from Boston Scientific Corporation for this study.

## Disclosure of conflict of interest

None.

**Address correspondence to:** Dr. Rainer Leuschke, Division of Healthcare Simulation, 1959 NE Pacific St, Suite T-293, Box #: 356410, Seattle, WA 98195, USA. Tel: 206-354-4873; E-mail: rainer@uw.edu

## References

[1] Auge BK, Pietrow PK, Lallas CD, Raj GV, Santa-Cruz RW and Preminger GM. Ureteral access sheath provides protection against elevated renal pressures during routine flexible ureteroscopic stone manipulation. J Endourol 2004; 18: 33-36.

[2] Croghan SM, Cunnane EM, O'Meara S, Muheilan M, Cunnane CV, Patterson K, Skolarikos A, Somani B, Jack GS and Forde JC. In vivo ureteroscopic intrarenal pressures and clinical outcomes: a multi-institutional analysis of 120 consecutive patients. Br J Urol 2023; 132: 531-540.

[3] Lildal SK, Hansen ESS, Laustsen C, Nørregaard R, Bertelsen LB, Madsen K, Rasmussen CW, Osther PJS and Jung H. Gadolinium-enhanced MRI visualizing backflow at increasing intra-renal pressure in a porcine model. PLoS One 2023; 18: e0281676.

[4] Noureldin YA, Kallidonis P, Ntasiotis P, Adamou C, Zazas E and Liatsikos EN. The effect of irrigation power and ureteral access sheath diameter on the maximal intra-pelvic pressure during ureteroscopy: in vivo experimental study in a live anesthetized pig. J Endourol 2019; 33: 725-729.

[5] Faure F, Duriez C, Delingette H, Allard J, Gilles B, Marchesseau S, Talbot H, Courtecuisse H, Bousquet G and Peterlik I. Sofa: a multi-model framework for interactive physical simulation. In: editors. Soft tissue biomechanical model-

ing for computer assisted surgery. Springer; 2012. pp. 283-321.
[6] Levillain A, Confavreux C, Decaussin-Petrucci M, Durieux E, Paparel P, Carval KLB, Maillard L, Bermond F, Mitton D and Follet H. Mechanical properties and structure of tumour microenvironment in breast, kidney, and thyroid cancer. 5th Int Cancer Symp 2022; 1p-1p.
[7] Mohammadi H and Sahai E. Mechanisms and impact of altered tumour mechanics. Nat Cell Biol 2018; 20: 766-774.
[8] Festas AJ, Ramos A and Davim JP. Medical devices biomaterials-A review. Proc Inst Mech Eng Pt L J Mater Des Appl 2020; 234: 218-228.
[9] Shen J and Roth S. Validation of rib structural responses under dynamic loadings using different material properties: a finite element analysis. Med Eng Phys 2022; 105: 103820.
[10] Zuckerman DM, Brown P and Nissen SE. Medical device recalls and the FDA approval process. Arch Intern Med 2011; 171: 1006-1011.
[11] Melvin J, Stalnaker RL, Roberts V and Trollope M. Impact injury mechanisms in abdominal organs. SAE Paper 1973.
[12] Farshad M, Barbezat M, Flüeler P, Schmidlin F, Graber P and Niederer P. Material characterization of the pig kidney in relation with the biomechanical analysis of renal trauma. J Biomech 1999; 32: 417-425.
[13] Zhang Z, Tan X, Li M, M W, Zeng S and Wu Y. Evaluation of the mechanical properties of porcine kidney. PLoS One 2024; 19: e0307778.
[14] Karimi A and Shojaei A. Measurement of the mechanical properties of the human kidney. IRBM 2017; 38: 292-297.
[15] Umale S, Deck C, Bourdet N, Dhumane P, Soler L, Marescaux J and Willinger R. Experimental mechanical characterization of abdominal organs: liver, kidney & spleen. J Mech Behav Biomed Mater 2013; 17: 22-33.
[16] Vuskovic V. Device for in-vivo measurement of mechanical properties of internal human soft tissues. ETH Zurich, 2001.
[17] Nava A, Mazza E, Kleinermann F, Avis NJ, McClure J and Bajka M. Evaluation of the mechanical properties of human liver and kidney through aspiration experiments. Technology and Health Care 2004; 12: 269-280.
[18] Urban MW, Rule AD, Atwell TD and Chen S. Novel uses of ultrasound to assess kidney mechanical properties. Kidney360 2021; 2: 1531-1539.
[19] Oratis AT, Subasic JJ, Hernandez N, Bird JC and Eisner BH. A simple fluid dynamic model of renal pelvis pressures during ureteroscopic kidney stone treatment. PLoS One 2018; 13: e0208209.
[20] Williams JG, Rouse L, Turney BW, Waters SL and Moulton DE. A lumped-parameter model for kidney pressure during stone removal. IMA J Appl Math 2020; 85: 703-723.
[21] Djurhuus JC, Saksø P and Mortensen J. The pressure-volume relationship of the pig renal pelvis. J Urol 1986; 135: 648-651.
[22] Rezakahn Khajeh N, Hall TL, Ghani KR and Roberts WW. Determination of irrigation flow-rate during flexible ureteroscopy: methods for calculation using renal pelvis pressure. J Endourol 2022; 36: 1405-1410.
[23] Rehman J, Monga M, Landman J, Lee DI, Felfela T, Conradie MC, Srinivas R, Sundaram CP and Clayman RV. Characterization of intrapelvic pressure during ureteropyeloscopy with ureteral access sheaths. Urology 2003; 61: 713-718.
[24] Kim HJ, Louters MM, Dau JJ, Hall TL, Ghani KR and Roberts WW. Quantification of outflow resistance for ureteral drainage devices used during ureteroscopy. World J Urol 2023; 41: 873-878.
[25] Marom R, Dau JJ, Hall TL, Ghani KR, Louters MM, Kim HJ, Khajeh NR and Roberts WW. Effect of outflow resistance on intrarenal pressure at different irrigation rates during ureteroscopy: in vivo evaluation. Urolithiasis 2023; 51: 98.
[26] Ciulla MG, Massironi A, Sugni M, Ensign MA, Marzorati S, Forouharshad M, Ciulla MG, Massironi A, Sugni M, Ensign MA, Marzorati S and Forouharshad M. Recent advances in the development of biomimetic materials. Gels 2023; 9: 833.
[27] Adams F, Qiu T, Mark A, Fritz B, Kramer L, Schlager D, Wetterauer U, Miernik A and Fischer P. Soft 3D-printed phantom of the human kidney with collecting system. Ann Biomed Eng 2017; 45: 963-972.
[28] O'Meara S, Cunnane EM, Croghan SM, Cunnane CV, Walsh MT, O'Brien FJ and Davis NF. Mechanical characteristics of the ureter and clinical implications. Nat Rev Urol 2024; 21: 197-213.
[29] Valverde MG, Mille LS, Figler KP, Cervantes E, Li VY, Bonventre JV, Masereeuw R and Zhang YS. Biomimetic models of the glomerulus. Nat Rev Nephrol 2022; 18: 241-257.
[30] Wang D, Gust M, Ferrell N, Wang D, Gust M and Ferrell N. Kidney-on-a-chip: mechanical stimulation and sensor integration. Sensors 2022; 22: 6889.
[31] Casarin M, Toniolo I, Todesco M, Carniel EL, Astolfi L, Morlacco A and Moro FD. Mechanical characterization of porcine ureter for the evaluation of tissue-engineering applications. Front Bioeng Biotechnol 2024; 12: 1412136.

[32] Shin J, Tabatabaei Rezaei N, Choi S, Li Z, Kim DH and Kim K. Photocrosslinkable kidney decellularized extracellular matrix-based bioink for 3D bioprinting. Adv Healthc Mater 2025; 14: 2501616.
[33] Fernandes NATC, Sharma S, Arieira A, Hinckel B, Silva F, Leal A, Carvalho Ó, Fernandes NATC, Sharma S, Arieira A, Hinckel B, Silva F, Leal A and Carvalho Ó. Experimental validation of time-explicit ultrasound propagation models with sound diffusivity or viscous attenuation in biological tissues using COMSOL multiphysics. Bioengineering 2025; 12: 946.
[34] Izdihar K, Razak HRA, Supion N, Karim MKA, Osman NH, Norkhairunnisa M, Izdihar K, Razak HRA, Supion N, Karim MKA, Osman NH and Norkhairunnisa M. Structural, mechanical, and dielectric properties of polydimethylsiloxane and silicone elastomer for the fabrication of clinical-grade kidney phantom. Appl Sci 2021; 11.
[35] Brant WE and Helms CA. Fundamentals of diagnostic radiology. Lippincott Williams & Wilkins, 2007.